Title: Dispersible oxygen microsensors map oxygen gradients in three-dimensional cell cultures.

Authors: Sasha Cai Lesher-Perez[1,2]; Ge-Ah Kim[2,3]; Chuan-hsien Kuo[1]; Brendan M. Leung[1,2]; Sanda Mong[1]; Taisuke Kojima[2,4]; Christopher Moraes, [1,2,5]; M. D. Thouless[3,6], Gary D. Luker[1,7,8,9]; Shuichi Takayama[1,2,4,10*]

Affiliation:

[1]Department of Biomedical Engineering, University of Michigan, Ann Arbor, USA
[2]Biointerfaces Institute, University of Michigan, Ann Arbor, USA
[3]Department of Materials Science and Engineering, University of Michigan, Ann Arbor, USA
[4]Department of Macromolecular Science and Engineering, University of Michigan, Ann Arbor, USA
[5]Department of Chemical Engineering, McGill University, Montreal, Canada
[6]Department of Mechanical Engineering, University of Michigan, Ann Arbor, USA
[7]Department of Radiology, University of Michigan School of Medicine, Ann Arbor, MI, USA
[8]Center for Molecular Imaging, Department of Radiology University of Michigan, Ann Arbor, MI, USA
[9]Department of Microbiology and Immunology, University of Michigan, Ann Arbor, USA
[10]Michigan Center for Integrative Research in Critical Care, University of Michigan, Ann Arbor, USA
* - corresponding author: takayama@umich.edu

Abstract

Phase fluorimetry, unlike the more commonly used intensity-based measurements, is not affected by differences in light paths from culture vessels, by optical attenuation through dense 3D cell cultures and hydrogels, and minimizes the dependence on signal intensity for accurate measurements. This work describes the use of phase fluorimetry on oxygen-sensor microbeads to perform oxygen measurements in different microtissue culture environments. In one example, cell spheroids were observed to deplete oxygen from the cell-culture medium filling the bottom of conventional microwells within minutes, whereas oxygen concentrations remained close to ambient levels for several days in hanging-drop cultures. By dispersing multiple oxygen-microsensors in cell-laden hydrogels, we also mapped cell-generated oxygen gradients. The spatial oxygen mapping was sufficiently precise to enable use of computational models of oxygen diffusion and uptake to give estimates of the cellular oxygen uptake rate and the half-saturation constant. The results show the importance of integrated design and analysis of 3D cell cultures from both a biomaterial and oxygen supply aspect. While this paper specifically tests spheroids and cell-laden gel cultures, the described methods should be useful for measuring pericellular oxygen concentrations in many different biomaterials and culture formats.

Key words: biocompatible oxygen microsensor, optical oxygen detection, spatial oxygen mapping, 3D tissue culture

Introduction

Three-dimensional (3D) cultures that use hydrogels[1] or specialized culture vessels are increasingly used to elicit more physiological cellular responses than are available from conventional 2D cultures[2–5]. Oxygenation within these tissue cultures is an important regulator of cell function. Physiological oxygen levels *in vivo* range from ~14% in lung alveoli down to ~3% in some tissues, such as muscle and skin (dermal papillae)[6]. Even lower levels of oxygen exist in tissues associated with different pathologies, such as tumors, ischemia, and obesity[7,8]. Re-creation of physiological oxygen levels in tissue cultures enables researchers to probe specific biological phenomena, in more representative microenvironments.

3D spheroid cultures are commonly used as a model system for avascular tumors[9] and other pathological tissues[10,11] . Spheroids have a diffusion-limited supply of critical nutrients such as oxygen, resulting in marked gradients within the tissue aggregate, mirroring oxygen gradients expected in avascular tumors[9,12]. Spheroids have remained popular models owing to their defined shape and structural architecture of a cell mass with a constant volume, which enables computational models to assess these structures radially, minimizing the complexity of modeling as compared to radially asymmetric systems[3,12]. Spheroids are formed in a broad array of methods that promote cell-cell attachment by limiting cell-substrate interaction. These methods, however, differ significantly in vessel types and hence oxygen-transfer properties. Specific examples of spheroid cultures include low-adhesion, curved wells[13], agarose-coated wells[14], microfluidic devices[15], honeycomb wells[16], and hanging-drop cultures[17].

While formation of oxygen gradients within spheroids is well-appreciated, there is often less emphasis on differences in oxygen levels in the surrounding culture medium that arise from using these different culture methods. This paper aims to fill this gap.

While a variety of oxygen sensors exist, intensity-based measurements of the sensors makes few, if any, of them meet the requirements for oxygen-evaluation gradient mapping of 3D cell cultures in being non-toxic to cells, non-tethered, microscale, and accurate. In particular, cell-compatible optical oxygen sensing microbeads reported previously[26,27] have been prone to inaccuracies owing to heterogeneities in the sensors[27,29] and inherent variabilities associated with intensity-based optical sensing modalities. Even ratiometric imaging with an oxygen-insensitive reference dye present is challenging, as photo-bleaching properties and excitation/emission properties will be different between the oxygen-sensitive and oxygen-independent dye. In contrast, measurement methods that depend on the indicator's luminescent lifetime, such as phase fluorimetric measurements[34,38,48], can usually eliminate inconsistencies that arise from intensity differences, caused by dye-loading variability, photobleaching, and optical path variability inherent to 3D tissues[48,49].Using small, dispersible polydimethylsiloxane (PDMS)-based oxygen sensing microbeads with phase fluorimetry [18,19] we quantified significant differences in oxygen microenvironments between three different but commonly-used 3D culture formats. Furthermore, for the cell-laden hydrogel culture, oxygen gradient maps were used

together with computer simulations to estimate the constants for the uptake rate of cellular oxygen and for the half-saturation of oxygen.

Methods and Materials

Microsensor Fabrication and Calibration

Briefly, lab-fabricated microsensors were generated by producing PDMS microbeads using a microfluidic flow-focusing device. PDMS beads were infused with tris(4,7-diphenyl-1,10-phenanthroline) ruthenium(II) dichloride and then calibrated over a range of pre-mixed combination of N_2 and O_2 gas spanning from 21% (room air) to 0% O_2. Phase-shift measurements were taken at each oxygen interval using a custom setup similar to that already described by others[20]. A more in-depth protocol for the fabrication and calibration of these microsensors can be found in SI Methods and Materials, with detailed information on the oxygen-sensing capability of our imaging setup.

Cell culture

Human embryonic kidney 293T (HEK 293T) cells (ATCC® CRL-1573™), HS-5 human bone-marrow stromal cells (ATCC® CRL-11882™), and MDA-MB-231 human breast-cancer cells that stably expressed eGFP (MDA-MB-231-eGFP) were cultured with Dulbecco's modified Eagle medium (Gibco, Carlsbad, CA, USA) supplemented with 10% fetal bovine serum (FBS) and 1% antibiotic-antimycotic. The medium was refreshed every 2 to 3 days, and the cultured cells were passaged using 0.25% Trypsin/EDTA (Gibco, Carlsbad, CA, USA) when sub-confluent, 70~80%. The cytotoxicity assessments were done with HS-5 cells. The experiments with spheroid cultures were done using HEK 293T cells. The cell-laden hydrogel work used to assess cell-generated oxygen gradients was performed using the MDA-MB 231 cells.

Assessing oxygen levels generated by spheroids in different culture formats

Spheroids were generated using high-throughput hanging-drop-array plates[21] and the culture methods recently presented[22]. Prior to use, a hydrophilic coating was applied onto the entire surface of the hanging-drop plate by soaking the plate overnight in 0.1%, Pluronic F108. The plate was then dried and sterilized by ultraviolet light before seeding with cells. To form the hanging drops, 25 μL of a cell suspension at a concentration of 2.0×10^5 HEK 293T cells/mL were pipetted through the access holes on the top-side of the plate, with the tip of each pipette being inserted into the access hole to guide the sample to the bottom surface. The cell-culture medium was supplemented with A4M MethoCel (Dow Chemical Co., Auburn Hills, MI, USA) at 0.024% (w/v). The spheroids formed over 24 hours. At this time microsensors were placed either into hanging drops with spheroids or into 96-well round-bottom microplate wells. The round-bottom microplate wells were then filled with 1, 5, 10 or 50 spheroids. Microsensors were also placed in media with only hanging drops and round-bottom wells as controls. The spheroids were monitored for a minimum of 18 hours in the different culture formats. A second study assessed hanging drops with 0, 1, 3, or 10 spheroids being placed into hanging drops containing microsensors. These systems were monitored at various stages over the course of a single day.

Mapping oxygen distribution in cell-patterned hydrogels

A more complete protocol to generate a spatially-patterned, cell-laden, collagen hydrogel surrounded by a cell-free collagen hydrogel has been previously described[23]. Briefly, spatial patterning was done by coating PDMS onto a glass slide, which was then covered with polyacrylamide. The polyacrylamide coating was selectively oxidized using a protective mask and applying plasma oxidation (Covance MP, FemtoScience, Hwaseong-si, Gyeonggi-do, South Korea). Trypsinized MDA-MB-231 eGFP cells were mixed with the oxygen microsensors and neutralized type-I bovine collagen (BD Biosciences, San Jose, CA, USA) to create a suspension of 1.0 x 10^7 cells/mL and 2 x 10^3 beads/mL in 2 mg/mL of collagen. 8 µL of this suspension were dispensed onto the adhesive pattern and allowed to polymerize for 45 minutes at 37 °C. The overlaying gel consisted of a suspension of oxygen microsensors 200 beads/mL in 2.5 mg/mL collagen. 250 µL were dispensed over the polymerized core region, and incubated at 37 °C for 1 hour to polymerize the overlaying gel. 2 mL of cell-culture media were added to each well, and the samples were cultured at 37 °C. Oxygen levels were measured after 24 hours of culturing (steady state), and then mapped radially, by using the distance from the center of the cell-laden region. The results from our system were compared with measurements using a commercially available Seahorse XF^e Extracellular Flux Analyzer and Ocean Optics NeoFox. Both the oxygen-consumption rate and oxygen levels within cells seeded in collagen gels were compared following similar protocols for processing cells and forming the collagen gel. A more in-depth description for these comparative measurements acquisition and measurements can be found in SI Methods and Materials.

Oxygen-depletion simulations

In order to model the cell-generated oxygen gradients, finite-element analyses were conducted using COMSOL Multiphysics® v5.1 Chemical Reaction Engineering Module (COMSOL, Inc., Burlington, MA). In the model, a two-dimensional axisymmetric geometry was used to mimic the actual experimental configuration, which consisted of a region composed of a cell-free hydrogel (6 mm radius and 1.8 mm height) encapsulating the cell-laden region (0.85 mm radius and 0.1 mm height), respectively referred to as region 1 and 2 in the Figure 5. The steady-state oxygen distribution within this geometry was studied assuming two mechanisms: diffusion and Michaelis-Menten kinetics. The governing equation[24] for such a system is

$$0 = D_{O2}\left[\frac{1}{r}\frac{\partial}{\partial r}\left(r\frac{\partial C_{O2}}{\partial r}\right) + \frac{\partial^2 C_{O2}}{\partial^2 z}\right] + \gamma, \quad (1)$$

where D_{O2} is the diffusivity of oxygen, C_{O2} is the oxygen concentration. It was assumed that the oxygen consumption activity, or reaction term (γ), only occurs in the cell-laden region (region 2) and is affected by the local oxygen concentration. This adaptive behavior for γ was simulated assuming Michaelis-Menten kinetics[25]:

$$\gamma = -V_{max}\left(\frac{C_{O2}}{K_m + C_{O2}}\right), \quad (2)$$

where V_{max} is the maximum oxygen-respiration rate, or oxygen uptake rate, and K_m is the concentration of oxygen at which the oxygen uptake rate decreases by one half. The diffusivity of O_2 in a cell-culture medium and in a collagen gel was assumed to be similar to that in water ($D_{O_2} = 2\times10^{-5}$ cm^2/s[26]), and it was assumed to be uniform throughout the geometry. The cell-free

region (region 1), is dominated only by diffusion, and the reaction term γ, is zero. The boundaries at the air/solid interface were assumed to have a continuous influx of O_2 to maintain a constant concentration of $c^*_{O_2}$ being determined by Henry's law:

$$c^*_{O_2} = p_{O_2} \cdot \mathrm{S} \quad (3)$$

where p_{O_2} is the oxygen partial pressure in air (p_{O_2} = 158.8 mmHg) and S is the solubility of oxygen in culture media ($S = 1.29\times10^{-3}$ mol/m^3 mmHg[27]). A dimensional analysis of the problem shows that the values of V_{max} and K_m scale with the assumed values of D_{O_2} and $c^*_{O_2}$, respectively, and that there are no other dimensionless groups with unknown parameters. Therefore, parametric sweeps using just these two variables were used to identify a range of values for V_{max} and K_m that resulted in a prediction that bracketed the experimental data.

Results

Oxygen monitoring in different spheroid culture platforms

The oxygen microsensors were calibrated using both intensity-based and phase-shift measurements. Phase fluorimetry showed a highly consistent response to different oxygen levels ranging from 0-21%, in contrast to intensity-based quenching (Figure SI 2A, C). To reduce the variation inherent in the microsensors, phase fluorimetry of our monodispersed oxygen microsensors was performed throughout this work. The microsensors were used to compare two different formats of spheroid cultures: hanging drops and 96-well round-bottom plates. The oxygen levels were measured after 18 hours for a single HEK 293T spheroid (5.0 x 10^3 cells/spheroid) in these two culture formats. The oxygen levels within spheroids in the hanging drop cultures did not change within 5 days (data not shown) when compared to the media controls without cell cultures (both hanging-drop, and round-bottom wells). However, the oxygen levels around the spheroids in round-bottom wells were lower (Figure 1). Since a significant drop in oxygen was measured in the microwell, even with just a single spheroid, the platform was investigated further to explore for effects of multiple spheroids. As seen in Figure 1, more spheroids (*e.g.*, one, five, ten, and fifty) resulted in lower steady-state (at 18 hr) oxygen levels. Figure 1C shows the ability to perform real-time, continuous monitoring of peri-tissue oxygen concentrations, as well as the spheroid number-dependence (1, 5, or 50 spheroids) of the rate of decrease in oxygen concentration in round-bottom wells. Figure 1D further highlights that the oxygen levels in hanging drop cultures do not exhibit a significant change as compared to media controls, even with 10 spheroids maintained in the hanging drops.

Oxygen gradient mapping and modeling of 3D hydrogel cultures

The oxygen microsensors were also dispersed into micropatterned cell-laden hydrogel constructs[23] (Figure 2A). Using phase fluorimetry, we observed oxygen concentrations to vary from hypoxic levels of ~0.5% O_2 (0.00496 mol/m^3) within the interior of the cell-laden region to higher oxygen levels in the cell-free regions of the hydrogel (Figure 2B). The oxygen profile was fit to a computational model (Figure 3A) with a two-dimensional axisymmetric geometry, where the best fits gave a V_{max} = (1.0±0.27) x 10^{-2} mol/m^3/s and K_m = (6.0±1.0) x 10^{-3} mol/m^3 (*i.e.*, 6.0±1.0 μM), (Figure 3B). Again, it is emphasized that these values are based on the

assumptions that $D_{O_2} = 2\times10^{-5}$ cm^2/s[26] and $c^*_{O_2} = 0.205$ mol/m^3, with V_{max} and K_m scaling with each parameter, respectively.

Discussion

Oxygen is important not only as a key substrate for respiration but also as a regulatory molecule that alters gene expression and cell function. Because oxygen is only sparingly soluble in aqueous solutions, with a reduced concentration as compared to that in the atmosphere, and because oxygen diffusion is relatively slow, pericellular oxygen concentrations can be significantly altered by uptake of oxygen by the cells themselves. 3D cell-culture platforms are particularly susceptible to such effects because of the high density of cells used compared to 2D cultures and diffusion-limited characteristics of these cultures. The wealth of new information from custom 3D cultures, which more aptly reconstruct aspects of the cellular microenvironment milieu has been well documented in recent years. Oxygen gradients through these 3D tissue is well recognized. On the other hand, oxygen gradients that can form in the pericellular microenvironment, is not as commonly appreciated. For example, spheroid cultures in non-stick microwell cultures are commonly used interchangeably with hanging-drop cultures as both form spheroids. In this work, we highlight the variation that can occur as a function of culture vessel-type or from the use of a gel-embedded culture format.

While a variety of oxygen sensors exist, we prepared custom, lab-fabricated oxygen sensors in a dispersible microbead format (Figure SI 1). A major reason is that cell-compatible optical oxygen sensing microbeads reported previously[28,29] are easily dispersible, and could be easily incorporated into different culture formats, but have been prone to inaccuracies owing to heterogeneities in the sensors[29,30] and to inherent variabilities associated with intensity-based optical-sensing modalities (Figure SI 2A). On the other hand, while phase fluorimetry-based oxygen sensors also exist commercially, they primarily are large patch-based sensors or very small nano-scale sensors which can be taken up by cells. By using phase fluorimetry with ~100 micron-sized sensor beads, we demonstrated tighter reproducibility and peri-cellular oxygen concentrations across the physiological range of oxygen concentrations (Figure SI 2C). Phase-fluorimetric measurements[18,20] are used to eliminate inconsistencies that arise from dye-loading variability[29], photobleaching, and optical-path variability inherent to 3D tissues[31], enabling a more robust measurement system than intensity-based imaging previously described with bead-based microsensors[28,29]. In addition to enhancing the reproducibility of our measurement system between batches, we identified a relatively long shelf life for the sensors (Figure SI 2D), eliminating the concern for the use of the sensors over the course of the present study. This was possible because phase-fluorimetry measurements minimizes the dependence on intensity, which drops over time in beads, as seen in Figure SI 2D, Figure SI 3, and Table SI 1).

Once validated, we used our microsensors to evaluate different 3D cell cultures. For cultures of the same size spheroid, we observed higher peri-cellular oxygen levels (similar to no-cell controls) in hanging-drop cultures, whereas round-bottom-microwell cultures showed significantly lower oxygen levels at 18 hours. We attribute these differences to the distance between the spheroids and the air-liquid interface (~0 mm for the hanging drops and ~4 mm for the microwells, a schematic of the different geometries can be found in Figure 1). Because of the

less efficient oxygen-transfer rate of microwells, an increase in cell mass (number of spheroids) led to even lower steady-state oxygen levels (Figure 1B), some of which approach hypoxic/anoxic levels[32–34]. This observation was in contrast to those observed by placing multiple spheroids in a hanging drop, which did not appear to significantly affect the oxygen levels in the hanging-drop cultures. These results highlight the need to evaluate the role of microculture vessel-type on oxygen transfer rates, as this may have a substantial impact on cell function.

We also mapped oxygen concentrations (Figure 2) within and around an island of cells patterned within a hydrogel. The MDA-MB 231 cells used for this portion of the study do not spontaneously form tight spheroids [22], enabling us to simulate a 2D slice of a spheroid in a 3D culture-like environment. Employing a prevalent practice for the qualification of bioreactors[35], we generated a computational model of oxygen supply, diffusion, and uptake (Figure 3) by using the geometry of the experimental system and a range of literature values of oxygen V_{max} and K_m [36–42] to run a parametric sweep. We approximated the best fit for V_{max} and K_m to be (1.06±0.27) x 10^{-2} mol/m^3/s and (6.0±1.0) x 10^{-3} mol/m^3 (i.e. (6.0±1.0) μM), respectively of MDA-MB-231 cells in our system. The value for V_{max} of 1.06 x 10^{-2} mol/m^3/s corresponds with an oxygen uptake rate of (3.00±0.10) x 10^{-17} mol/cell/s which falls between previously reported values [39] (1.6 x 10^{-17} mol/cell/s while in suspension and 5.6 x 10^{-17} mol/cell/s while in a monolayer culture). Commercially available systems were also used to determine the oxygen consumption rate (OCR) and the oxygen levels in uniform, unpatterned cell-laden hydrogel culture formats. The Seahorse XF^e Extracellular Flux Analyzer gave an oxygen-consumption rate (OCR) for MDA-MB-231 cells in a uniform collagen gel of 271.63±2.72 pmol/min. This corresponds to an oxygen-uptake rate of (1.30 ±.013) x 10^{-17} mol/cell/s (Figure SI 5). This is very similar to our computationally produced values, given the differences in the culturing format. Oxygen levels were measured by Ocean Optics NeoFox within DMEM for a blank collagen gel, and cell-laden collagen gels. When using the probe, all the measurements had to be end-point measurements within the collagen gel, since the ~ 700 μm probe tore through the gel as it was inserted. Additionally, the culture disruption and the relatively large size of the probes made accurate measurements difficult, and detailed mapping of oxygen gradients impossible. This highlights two benefits of using untethered microsensing probes, such as those presented within this work.

While there are a number of other papers on evaluating oxygen measurements for cell, tissue and organismal cultures[43–48], this analysis is one of the few that has pursued sufficient accuracy and resolution, in terms of both oxygen levels and position of the measurements, to allow estimations of the rate of uptake of cellular oxygen. This method also has advantages over the more conventional Clark electrodes in not consuming oxygen during the measurements, and being less destructive in nature than Clark electrodes and other fiber-based probes[36,37,44,49].

Conclusions

The recent increase in the use of 3D cell cultures presents new challenges in understanding and regulating cellular oxygen microenvironments. We implemented non-toxic, dispersible, optical oxygen-sensing microbeads and used phase fluorimetry, rather than the more common fluorescence intensity-based methods, to accurately quantify pericellular oxygen concentrations. This sensing strategy was used to show that hanging drop spheroid cultures maintain pericellular

oxygen levels very similar to atmospheric oxygen levels while microwell spheroid cultures lead to reduced oxygen levels in a time- and cell mass-dependent manner. Furthermore, the method was used to provide a high-resolution map of oxygen levels in and around a hydrogel-embedded 3D cell culture. Computational modeling and curve fitting of the observed oxygen gradient provided cell specific parameters for the oxygen uptake rate, V_{max} and K_m[38,39]. The results provide a cautionary note for interchangeable use of different methods to form and culture spheroids, even if the spheroid size and shape appear the same. Furthermore, we envision the oxygen microsensors and optical detection protocols to be useful in mapping oxygen gradients in a broad range of culture systems such as bioreactors, organoid cultures, and 3D organ-on-a-chip systems.

Conflict of Interests

No conflict of interest.

Acknowledgements

This material is based upon work supported by the NIH (CA170198, AI116482) and the Defense Threat Reduction Agency (DTRA) and Space and Naval Warfare Command Pacific (SSC PACIFIC) under Contract No. N66001-13-C-2027 INteGrated Organoid Testing System (INGOTS), Wake Forest University. Support for some of the early development of the microspheres was provided by NSF (CMMI-0700232). Any opinions, findings and conclusions or recommendations expressed in this material are those of the author(s) and do not necessarily reflect the views of the DTRA and SSC PACIFIC. SCLP was supported by an NSF Graduate Research Fellowship Program (DGE 1256260; ID: 2011101670) and the NIH Cellular Biotechnology Training Program (NIH GM008353). CM was supported by a Banting postdoctoral fellowship from the Natural Sciences and Engineering Research Council of Canada. TK thanks Yoshida Scholarship. The authors would also like to thank Dr. Joseph M. Labuz for useful discussion and thoughtful input, Priyan Weerappuli for help with MATLAB image processing, and Usha Kadiyala from J. Scott VanEpps lab (University of Michigan) and Prof. Joe Lo lab (University of Michigan) for the commercial O_2 sensor measurements.

References

1. Pampaloni, F., Reynaud, E. G. & Stelzer, E. H. K. The third dimension bridges the gap between cell culture and live tissue. *Nat. Rev. Mol. Cell Biol.* **8,** 839–845 (2007).
2. Moraes, C., Mehta, G., Lesher-Perez, S. C. & Takayama, S. Organs-on-a-Chip: A Focus on Compartmentalized Microdevices. *Ann. Biomed. Eng.* **40,** 1211–1227 (2011).
3. Leung, B. M. *et al.* Microscale 3D Collagen Cell Culture Assays in Conventional Flat-Bottom 384-Well Plates. *J. Lab. Autom.* 2211068214563793 (2014). doi:10.1177/2211068214563793
4. Brennan, M. D., Rexius-Hall, M. L., Elgass, L. J. & Eddington, D. T. Oxygen control with microfluidics. *Lab. Chip* **14,** 4305–4318 (2014).
5. Rexius-Hall, M. L., Mauleon, G., Malik, A. B., Rehman, J. & Eddington, D. T. Microfluidic platform generates oxygen landscapes for localized hypoxic activation. *Lab. Chip* **14,** 4688–4695 (2014).
6. Carreau, A., Hafny-Rahbi, B. E., Matejuk, A., Grillon, C. & Kieda, C. Why is the partial oxygen pressure of human tissues a crucial parameter? Small molecules and hypoxia. *J. Cell. Mol. Med.* **15,** 1239–1253 (2011).
7. Hosogai, N. *et al.* Adipose Tissue Hypoxia in Obesity and Its Impact on Adipocytokine Dysregulation. *Diabetes* **56,** 901–911 (2007).
8. Trayhurn, P. Hypoxia and Adipose Tissue Function and Dysfunction in Obesity. *Physiol. Rev.* **93,** 1–21 (2013).
9. Hirschhaeuser, F. *et al.* Multicellular tumor spheroids: An underestimated tool is catching up again. *J. Biotechnol.* **148,** 3–15 (2010).
10. Turner, P. A., Tang, Y., Weiss, S. J. & Janorkar, A. V. Three-Dimensional Spheroid Cell Model of In Vitro Adipocyte Inflammation. *Tissue Eng. Part A* **21,** 1837–1847 (2015).

11. Choi, Y. J., Park, J. & Lee, S.-H. Size-controllable networked neurospheres as a 3D neuronal tissue model for Alzheimer's disease studies. *Biomaterials* **34,** 2938–2946 (2013).

12. Mehta, G., Hsiao, A. Y., Ingram, M., Luker, G. D. & Takayama, S. Opportunities and challenges for use of tumor spheroids as models to test drug delivery and efficacy. *J. Controlled Release* **164,** 192–204 (2012).

13. Howes, A. L., Richardson, R. D., Finlay, D. & Vuori, K. 3-Dimensional Culture Systems for Anti-Cancer Compound Profiling and High-Throughput Screening Reveal Increases in EGFR Inhibitor-Mediated Cytotoxicity Compared to Monolayer Culture Systems. *PLoS ONE* **9,** (2014).

14. Casey, R. C. *et al.* β1-Integrins Regulate the Formation and Adhesion of Ovarian Carcinoma Multicellular Spheroids. *Am. J. Pathol.* **159,** 2071–2080 (2001).

15. Hsiao, A. Y. *et al.* Microfluidic system for formation of PC-3 prostate cancer co-culture spheroids. *Biomaterials* **30,** 3020–3027 (2009).

16. Lee, G., Lee, J., Oh, H. & Lee, S. Reproducible Construction of Surface Tension-Mediated Honeycomb Concave Microwell Arrays for Engineering of 3D Microtissues with Minimal Cell Loss. *PLOS ONE* **11,** e0161026 (2016).

17. Tung, Y.-C. *et al.* High-throughput 3D spheroid culture and drug testing using a 384 hanging drop array. *The Analyst* **136,** 473–478 (2011).

18. McDonagh, C. *et al.* Phase fluorometric dissolved oxygen sensor. *Sens. Actuators B Chem.* **74,** 124–130 (2001).

19. Holst, G. A., Köster, T., Voges, E. & Lübbers, D. W. FLOX—an oxygen-flux-measuring system using a phase-modulation method to evaluate the oxygen-dependent fluorescence lifetime. *Sens. Actuators B Chem.* **29,** 231–239 (1995).

20. Mehta, G. *et al.* Hard Top Soft Bottom Microfluidic Devices for Cell Culture and Chemical Analysis. *Anal. Chem.* **81,** 3714–3722 (2009).

21. Tung, Y.-C. *et al.* High-throughput 3D spheroid culture and drug testing using a 384 hanging drop array. *Analyst* **136,** 473–478 (2011).

22. Leung, B. M., Lesher-Perez, S. C., Matsuoka, T., Moraes, C. & Takayama, S. Media additives to promote spheroid circularity and compactness in hanging drop platform. *Biomater. Sci.* **3,** 336–344 (2015).

23. Kojima, T., Moraes, C., Cavnar, S. P., Luker, G. D. & Takayama, S. Surface-templated hydrogel patterns prompt matrix-dependent migration of breast cancer cells towards chemokine-secreting cells. *Acta Biomater.* **13,** 68–77 (2015).

24. Mattei, G., Giusti, S. & Ahluwalia, A. Design Criteria for Generating Physiologically Relevant In Vitro Models in Bioreactors. *Processes* **2,** 548–569 (2014).

25. Casciari, J. J., Sotirchos, S. V. & Sutherland, R. M. Variations in tumor cell growth rates and metabolism with oxygen concentration, glucose concentration, and extracellular pH. *J. Cell. Physiol.* **151,** 386–394 (1992).

26. Himmelblau, D. M. Diffusion of Dissolved Gases in Liquids. *Chem. Rev.* **64,** 527–550 (1964).

27. Morsiani, E. *et al.* Long-term expression of highly differentiated functions by isolated porcine hepatocytes perfused in a radial-flow bioreactor. *Artif. Organs* **25,** 740–748 (2001).

28. Jiang, K., Thomas, P. C., Forry, S. P., DeVoe, D. L. & Raghavan, S. R. Microfluidic synthesis of monodisperse PDMS microbeads as discrete oxygen sensors. *Soft Matter* **8,** 923–926 (2012).

29. Wang, L., Acosta, M. A., Leach, J. B. & Carrier, R. L. Spatially monitoring oxygen level in 3D microfabricated cell culture systems using optical oxygen sensing beads. *Lab. Chip* **13,** 1586 (2013).

30. Zhang, Y. S. *et al.* A cost-effective fluorescence mini-microscope for biomedical applications. *Lab. Chip* **15,** 3661–3669 (2015).

31. Welch, A. J., Yoon, G. & Van Gemert, M. J. C. Practical models for light distribution in laser-irradiated tissue. *Lasers Surg. Med.* **6,** 488–493 (1987).

32. Mueller-Klieser, W. Method for the determination of oxygen consumption rates and diffusion coefficients in multicellular spheroids. *Biophys. J.* **46,** 343–348 (1984).

33. Acker, H., Carlsson, J., Mueller-Klieser, W. & Sutherland, R. M. Comparative pO2 measurements in cell spheroids cultured with different techniques. *Br. J. Cancer* **56,** 325–327 (1987).

34. Kunz-Schughart, L. A., Kreutz, M. & Knuechel, R. Multicellular spheroids: a three-dimensional in vitro culture system to study tumour biology. *Int. J. Exp. Pathol.* **79,** 1–23 (1998).

35. Kirk, T. V. & Szita, N. Oxygen Transfer Characteristics of Miniaturized Bioreactor Systems. *Biotechnol. Bioeng.* **110,** 1005–1019 (2013).

36. Mueller-Klieser, W. F. & Sutherland, R. M. Influence of Convection in the Growth Medium on Oxygen Tensions in Multicellular Tumor Spheroids. *Cancer Res.* **42,** 237–242 (1982).

37. Radisic, M. *et al.* Oxygen gradients correlate with cell density and cell viability in engineered cardiac tissue. *Biotechnol. Bioeng.* **93,** 332–343 (2006).

38. Chunta, J. L., Vistisen, K. S., Yazdi, Z. & Braun, R. D. Uptake Rate of Cationic Mitochondrial Inhibitor MKT-077 Determines Cellular Oxygen Consumption Change in Carcinoma Cells. *PLoS ONE* **7,** e37471 (2012).

39. Wagner, B. A., Venkataraman, S. & Buettner, G. R. The Rate of Oxygen Utilization by Cells. *Free Radic. Biol. Med.* **51,** 700–712 (2011).

40. Jones, C. I. *et al.* Endothelial cell respiration is affected by the oxygen tension during shear exposure: role of mitochondrial peroxynitrite. *Am. J. Physiol. - Cell Physiol.* **295,** C180–C191 (2008).

41. Chandel, N. S., Budinger, G. R. S., Choe, S. H. & Schumacker, P. T. Cellular Respiration during Hypoxia ROLE OF CYTOCHROME OXIDASE AS THE OXYGEN SENSOR IN HEPATOCYTES. *J. Biol. Chem.* **272,** 18808–18816 (1997).

42. Zhao, F. *et al.* Effects of Oxygen Transport on 3-D Human Mesenchymal Stem Cell Metabolic Activity in Perfusion and Static Cultures: Experiments and Mathematical Model. *Biotechnol. Prog.* **21,** 1269–1280 (2005).

43. Westphal, I. *et al.* Oxygen mapping: Probing a novel seeding strategy for bone tissue engineering. *Biotechnol. Bioeng.* n/a-n/a (2016). doi:10.1002/bit.26202

44. Kellner, K. *et al.* Determination of oxygen gradients in engineered tissue using a fluorescent sensor. *Biotechnol. Bioeng.* **80,** 73–83 (2002).

45. Super, A. *et al.* Real-time monitoring of specific oxygen uptake rates of embryonic stem cells in a microfluidic cell culture device. *Biotechnol. J.* **11,** 1179–1189 (2016).

46. Yasukawa, T. *et al.* Detection of the Oxygen Consumption Rate of Migrating Zebrafish by Electrochemical Equalization Systems. *Anal. Chem.* **86,** 304–307 (2014).

47. Date, Y. *et al.* Monitoring oxygen consumption of single mouse embryos using an integrated electrochemical microdevice. *Biosens. Bioelectron.* **30,** 100–106 (2011).

48. Takahashi, R. *et al.* Noninvasively measuring respiratory activity of rat primary hepatocyte spheroids by scanning electrochemical microscopy. *J. Biosci. Bioeng.* **117,** 113–121 (2014).

49. Malda, J. *et al.* Oxygen gradients in tissue-engineered PEGT/PBT cartilaginous constructs: measurement and modeling. *Biotechnol. Bioeng.* **86,** 9–18 (2004).

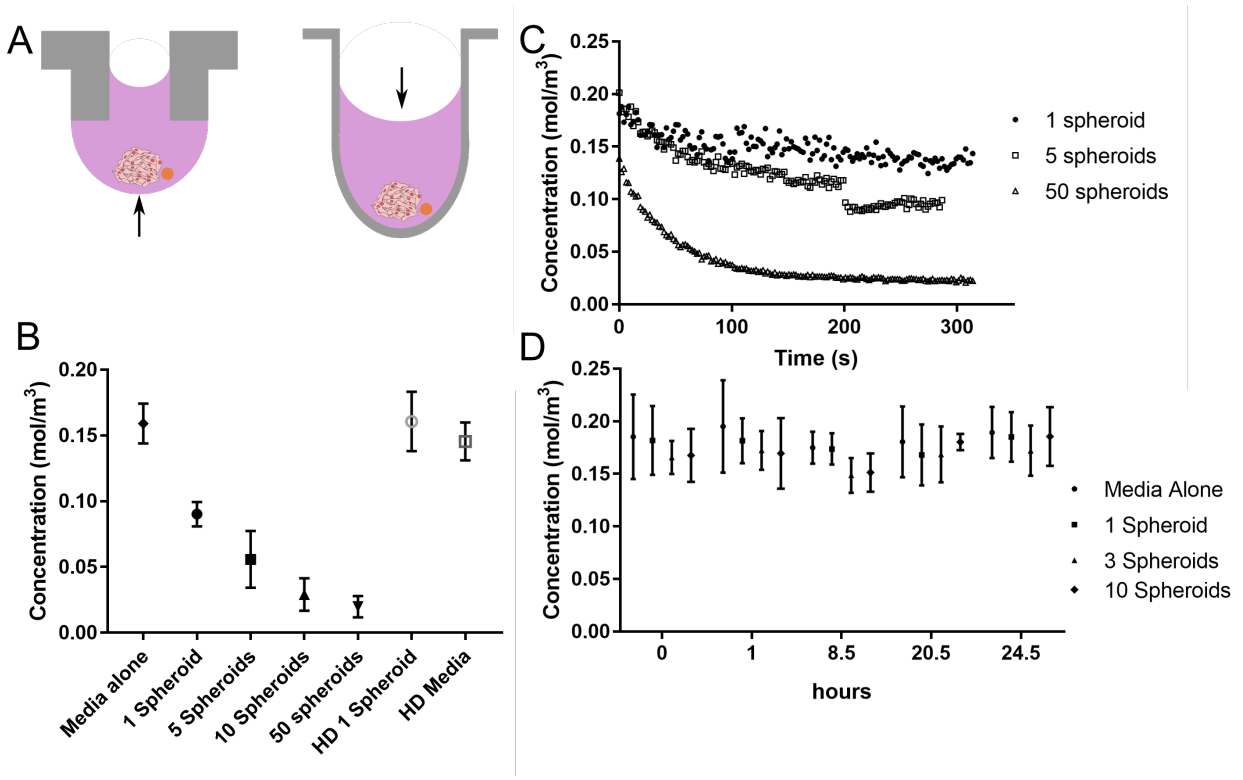

Figure 1. *Oxygen levels as a function of cell mass and culture vessel*. A) Schematic illustration of the hanging-drop (left) and round-bottom (right) spheroid-culture systems. These schematics illustrate a single spheroid with oxygen microsensor, to highlight the difference in culture geometries and spheroid position with respect to the air-liquid interface. Black arrows identify the air-liquid interface at the closest point to the spheroids. B) Microsensors were placed into 96 round-bottom wells with 0 (media control), 1, 5, 10, or 50 spheroids or into hanging drops (HD) with one spheroid or just media (control). Samples were observed over 18 hours with the stabilized oxygen values presented for 18 hours. Oxygen measurements were averaged per sample well together regardless of microsensor position in regards to cell mass to generate an oxygen level per well, error bars presented are one standard deviation, $n = 4$ well samples assessed per condition. C) Oxygen levels monitored in a microplate well after mixing and aeration of media followed by static culture, demonstrating real-time continuous measurement capability of the microsensors. D) Microsensors were placed into HD with 0 (media control), 1, 3, 10 spheroids, and monitored over the course of one day. Error bars presented are one standard deviation, a minimum of 3 samples were assessed per condition.

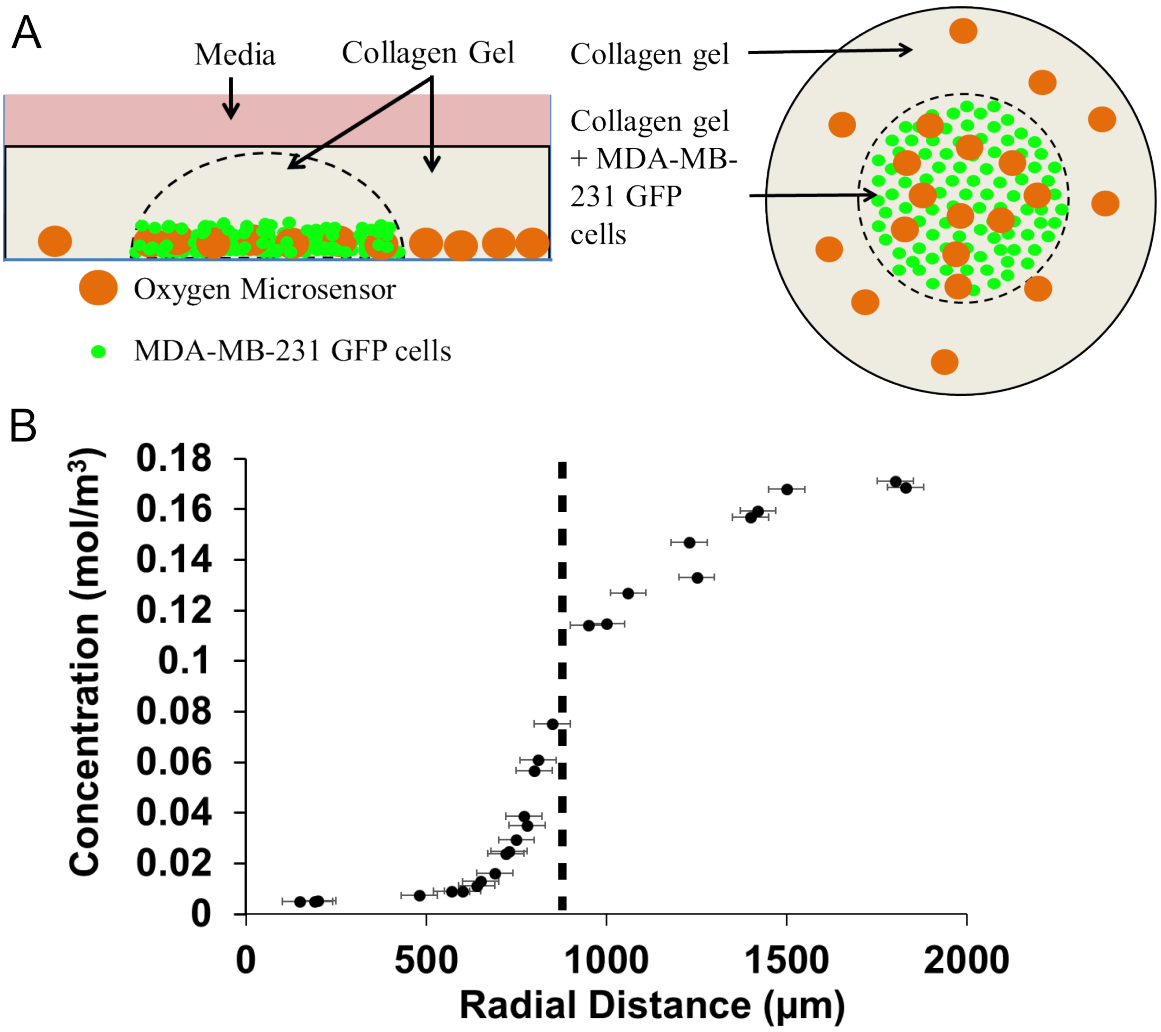

Figure 2. *Mapping cell-generated oxygen gradients in a hydrogel*. A) Side and top-down view schematic (not to scale) of the tissue culture with patterned MDA-MB-231 GFP cells. The spatially patterned culture consists of a cell-laden hydrogel core that is enveloped by a cell-free overlaying gel. Microsensors are dispersed within the two hydrogel regions. B) Phase-fluorimetric oxygen measurements throughout the hydrogel. The cell-laden/-free border is demarcated by the dotted line at a radial position of 850 μm. Measurements were plotted as a radial position from the center of the cell culture. The measurements were taken at a height of approximately 50 μm above the bottom of the culture system. We assumed the measurements obtained were an averaged measurement corresponding to the average oxygen level throughout the microsensors. As we are unable to exactly state the discrete point of the specific oxygen value, we used horizontal error bars to represent the location of the 100 μm sensors.

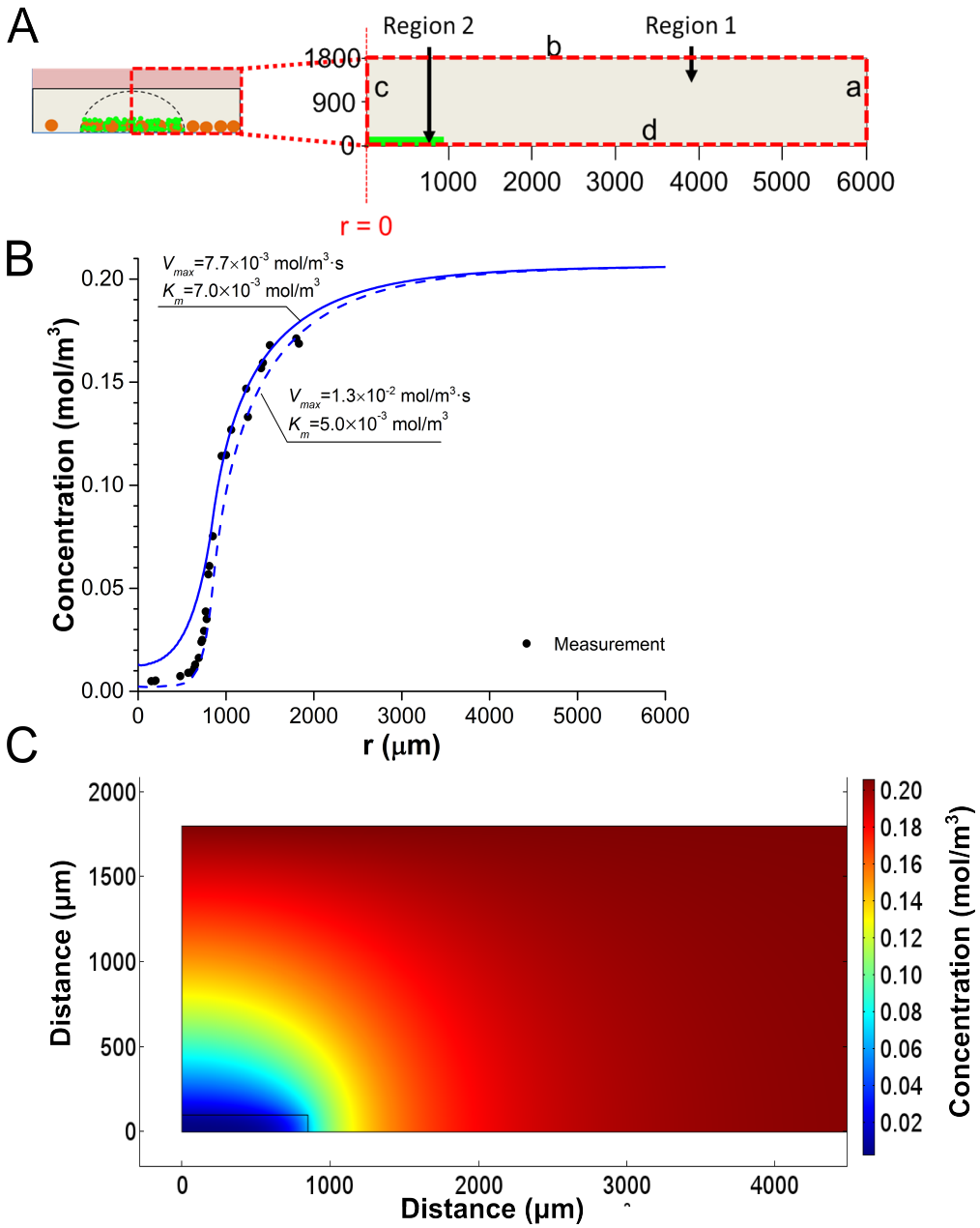

Figure 3. *Computer-simulated oxygen profile of micropatterned cell culture in a hydrogel*. A) Schematic representation of the two-dimensional axisymmetric geometry used for simulation of the hydrogel culture. Boundaries (a) and (d) represent PDMS-, and polystyrene-hydrogel interfaces, respectively. Boundary (b) represents cell culture media-air interface. Boundary (c) represents the *z-axis* at a radial position of 0, in the disk-shaped hydrogel. Region 1, and 2 represent the cell-free hydrogel plus cell culture media, and cell-laden hydrogel regions, respectively. B) Theoretical simulation of the oxygen profile with experimental data bracketed by the best fit for V_{max} and K_m of (1.0±0.27) x 10^{-2} mol/m^3/s and (6.0±1.0) x 10^{-3} mol/m^3, respectively. C) A 2D oxygen-concentration map of the hydrogel.